IEEE Access
Multidisciplinary | Rapid Review | Open Access Journal

Received June 2, 2019, accepted June 19, 2019, date of publication June 26, 2019, date of current version July 25, 2019.

Digital Object Identifier 10.1109/ACCESS.2019.2924931

Robust Optimization for Micromachine Design Problems Involving Multimodal Distributions

Z. L. HUANG[1], J. W. ZHANG[1], TARUN KUMAR[2], T. G. YANG[1], S. G. DENG[1], AND F. Y. LI[3]

[1]School of Mechanical and Electrical Engineering, Hunan City University, Yiyang 413002, China
[2]Department of Electronics and Electrical Communication Engineering, IIT Kharagpur, Kharagpur 721302, India
[3]College of Automotive and Mechanical Engineering, Changsha University of Science and Technology, Changsha 410114, China

Corresponding author: F. Y. Li (lfy703@sina.com)

This work was supported in part by the Major Program of National Natural Science Foundation of China under Grant 51490662, in part by the Educational Commission of Hunan Province of China under Grant 18A403 and Grant 17A036, and in part by the Natural Science Foundation of Hunan Province of China under Grant 2016JJ2012, Grant 2017JJ2022, and Grant 2019JJ40296.

ABSTRACT The conventional robust optimization methods usually focus on problems with unimodal random variables. In real applications, input random variables may follow multimodal distributions with multiple peaks in their probability density. When multimodal random variables are involved, the conventional methods, such as the mean-variance-based methods, will be not accurate. This paper presents an efficient robust optimization method, which provides a potential computational tool for engineering problems involving multimodal random variables. A robustness metric is formulated by introducing the concept of accepting/rejecting the limit to calculate the failure probability of the performance response, which can directly capture the multimodal characteristics of the performance. A second-order higher moment method is presented to efficiently conduct the probability calculation in the inner loop of design optimization. The proposed decoupling strategy drives the probability calculation and the design optimization sequentially and alternately. This method is applied to the three micromachine design problems, including a sweat-rate sensor, a piezoelectric sensor, and an image sensing module. The numerical results show that the method has excellent engineering practicality due to the comprehensive performance in terms of efficiency, accuracy, and convergence.

INDEX TERMS Probabilistic model, multimodal distribution, robust optimization, micromachine design.

I. INTRODUCTION

In the last several decades, the engineering optimization [1], [2] aimed at improving product cost-performance ratio has made significant progress in theory and method and has been widely used in practice. The conventional engineering optimization is usually based on deterministic parameters and models, and it can be solved by classical deterministic algorithms. In practical engineering problems, however, there exist various uncertainties in terms of structure sizes, material properties, and operating conditions. Although these uncertainties are small in most cases, they may cause product performance to fluctuate greatly or even fail. Due to the input uncertainties, the actual performance values fluctuate around its designed nominal value. Such fluctuation leads to the quality loss of the product. Robust optimization [3] can ensure that the key performance of a product accurately in the presence of uncertainties. The tasks of the robust optimization are to minimize 1) the deviation from the performance nominal value to the targeted value, and 2) the fluctuation of the actual performance value. The concept of robust optimization has been rooted in engineering design, and widely applied to various fields, such as electronic [4], vehicle [5], aerospace [6], and civil engineering [7]. Before performing the robust optimization, a method should be select to model the uncertainties [8], [9]. If sufficient sample data about the uncertain parameters are available to define their precise probability distribution, the probabilistic method [10], [11] is the prior choice. In this case, the input uncertainties are treated as the random variables; also, the product performance becomes a random function. As a result, its expectation can measure the robustness and should be minimized. The expectation generally consists of two terms, which are the square of the deviation of the performance mean value

The associate editor coordinating the review of this manuscript and approving it for publication was Wei Wei.

from its target and the variance of the performance value [12]. By robust optimization, the mean of the performance value is brought to its target, and simultaneously, the variation in the performance is minimized. The probabilistic-model-based robust optimization has achieved significant progress in methodology and applications. The different approaches to perform robust optimization in practice are reviewed in the lectures [13]–[15].

Most of the robust optimization methods handle problems with unimodal random variables. This means that the probability density function (PDF) of each random variable has only one mode (local maximum). In engineering optimization problems, however, the random variable may follow the distribution with two or more probability density modes, which is named as the multimodal random variable in this paper. For example, the long-term monitoring data verifies that the structural fatigue stress of a steel bridge carrying both highway and railway traffic follows a bimodal distribution [16]. The statistical results show that the Knoop microhardness of nanostructured partially stabilized zirconia coatings follows a bimodal distribution [17]. The abrupt local change of voltage in the complex power grid was pronounced to follow a bimodal distribution [18]. It was reported that the multimodal distribution exists in the vibratory load of a blade subject to stochastic dynamic excitation [19]. Similar to general problems, the multimodal problems can be solved by the classical probability methods, such as the first order second moment (FOSM) method [20], [21] and the most-probable-point-based (MPP-based) method [22], [23]. However, these methods suffer from accuracy problems. In these methods, each multimodal variable usually requires to be transformed into the standard normal random variable. This transformation makes the performance function much more nonlinear, and thus, the computational error may increase greatly. To handle the multimodal distributed problems in a better way, a few researches have been conducted. He et al. [19] formulated an asymptotic analysis cycle by establishing the optimal weighting scheme for the Laplace approximation of the random variable with the multimodal distribution. Hu and Du [24] employed the reliability methods based on first-order saddlepoint approximation to perform the uncertainty analysis for problems following bimodal distribution.

The two aforementioned methods are mainly applicable to the reliability assessment. However, it is not suitable to introduce them directly into the robust optimization for problems with multimodal distributions. There are two main reasons, one of which is still the accuracy problem. For example, when the PDF is highly unsymmetrical at modes, a large error is expected for the Laplace approximation [25]. The saddlepoint approximation method linearizes the performance function, which may fail to provide satisfying computational accuracy when the response function is highly nonlinear [26]. In robust optimization, performance robustness analysis is required at each design point. Its poor accuracy may result in an invalid result or even no convergence. On the other hand, even if the existing methods accurately obtain the mean and variance of the performance, they may fail to capture the multimodal feature and be not accurate to measure the performance robustness. Therefore, the development of an effective robust optimization method is of vital importance for the product design problems with multimodal distributions. To the best of our knowledge, such work has not yet been reported.

In the past two decades, performance optimization for micromachine systems has been extensively studied in both academic and engineering practice [27]. Given that uncertainties are inevitable in actual micromachine systems, robust optimization for uncertain micromachine systems has been explored [28]. In real applications, some input random variables may follow multimodal distributions. Conventional robust optimization method encounters a specific predicament. In this paper, a robust optimization model and an efficient algorithm are proposed, which provides a computational tool for the robust optimization with multimodal random variables. The proposed method is applied to the problems of micromachine design, in which the engineering practicability is discussed. The contents of this paper are organized as follows. The uncertainty modeling of input multimodal random variables is conducted using a Gaussian mixture model in Section 1. Then, the robust optimization model is formulated in Section 2. The corresponding algorithm is proposed in Section 3. In Section 4, this method has been validated through three engineering applications, including a sweat-rate sensor, a piezoelectric sensor, and an image sensing module. The conclusions have been shown in Section 5.

II. THE MODELLING OF INPUT MULTIMODAL RANDOM VARIABLES

The formulation of a probabilistic model for the input uncertainties is the prerequisite of a robust optimization using probability theory. The probabilistic modeling usually involves two steps. Firstly, a mathematical structure needs to be defined to describe uncertainty. The second step is to determine the parameter values of the mathematical structure. As a mathematical tool for describing random variables, the Gaussian mixture model (GMM) [29] is flexible enough and has been applied in various fields, such as machine learning, pattern recognition, etc. In this paper, the GMM is employed to formulate the input multimodal random variables of an uncertain problem. The PDF of a multimodal random variable can be written as the linear combination of multiple Gaussian components:

$$\rho_Z = \sum_{l=1}^{n_\varphi} \alpha_l \varphi\left(Z \,|\mu_l, \sigma_l\right)$$
$$\varphi = \frac{1}{\sqrt{2\pi}\sigma_l} \exp\left(-\frac{(Z-\mu_l)^2}{2\sigma_l^2}\right) \tag{1}$$

where Z denotes the random variable, φ is the i-th Gaussian component, n_φ is the number of the components, and α_l is the weight factor of the component. Each weight factor satisfies $\alpha_l > 0$ and $\sum_{l=1}^{n_\varphi} \alpha_l = 1$. The parameters to be

TABLE 1. The PDFs of the random responses in the distribution thpes.

Distribution types	PDF of f with $\mu_f = 3.0$, $\sigma_f^2 = 0.32$
Normal	$\rho_f = \varphi\left(f \mid 3.0, 0.57\right)$
Lognormal	$\rho_f = \dfrac{1}{0.57 \cdot \sqrt{2\pi} \cdot f} \exp\left(-\dfrac{\left(\ln f - 3.0\right)^2}{2 \cdot \left(0.57\right)^2}\right)$
Extreme value	$\rho_f = \dfrac{1}{0.57} \exp\left(\dfrac{\delta - 3.0}{0.57}\right) \exp\left(-\exp\left(\dfrac{\delta - 3.0}{0.57}\right)\right)$
Bimodal	$\rho_\delta = 0.30 \cdot \varphi\left(f \mid 1.8, 0.4\right) + 0.70 \cdot \varphi\left(f \mid 3.5, 0.3\right)$

determined in Equation (1) can be collected into the vector $\boldsymbol{\theta} = \left(\alpha_1, \mu_1, \sigma_1, \alpha_2, \mu_2, \sigma_2, \ldots, \alpha_{n_\varphi}, \mu_{n_\varphi}, \sigma_{n_\varphi}\right)$.

The maximum likelihood estimation method [30] is a common choice for parameter estimation. Given the observed samples $\boldsymbol{z} = \left(z_1, z_2, \ldots, z_{n_S}\right)$, a set of latent variables $\boldsymbol{\gamma} = \left\{\boldsymbol{\gamma}_1, \boldsymbol{\gamma}_2, \ldots, \boldsymbol{\gamma}_{n_S}\right\}$ is introduced, which indicates that the sample z_i was produced by the i-th Gaussian component. Each latent variable is a binary vector $\boldsymbol{\gamma}_i = \left(\gamma_{i,1}, \gamma_{i,2}, \ldots, \gamma_{i,n\varphi}\right)$, where $\gamma_{i,l} = 1$ and $\gamma_{i,p} = 0$ for $l \neq p$. Based on this, the log-likelihood function can be established as

$$\begin{aligned} \log \rho_Z\left(\boldsymbol{z}, \boldsymbol{\gamma} \mid \boldsymbol{\theta}\right) &= \log \prod_{i=1}^{n_S} \rho_Z\left(z_i, \boldsymbol{\gamma}_i \mid \boldsymbol{\theta}\right) \\ &= \sum_{i=1}^{n_S} \sum_{l}^{n_\varphi} \gamma_{i,l} \log\left(\alpha_l \varphi\left(z_i \mid \mu_l, \sigma_l\right)\right) \end{aligned} \tag{2}$$

The parameter vector $\boldsymbol{\theta}$ can be searched by maximizing the log-likelihood function:

$$\max_{\boldsymbol{\theta}} \ \log \rho_Z\left(\boldsymbol{z}, \boldsymbol{\gamma} \mid \boldsymbol{\theta}\right) \tag{3}$$

The expectation maximization algorithm [31] is employed to solve the optimization problem of Equation (3) in this paper.

III. THE MODELLING OF INPUT MULTIMODAL RANDOM VARIABLES

When an uncertainty problem involves multimodal distribution, the random response will mostly exhibit the multimodal feature. The classical robust optimization based on probabilistic models uses the mean and variance of the random response to measure the robustness of product performance under certainties. This robustness metric is generally sufficient for unimodal responses, but it may fail to grasp the multimodal characteristics of performance response. For example, FIGURE 1 shows the four random responses with the same mean $\left(\mu_f = 3\right)$ and variance $\left(\sigma_f^2 = 0.32\right)$, which

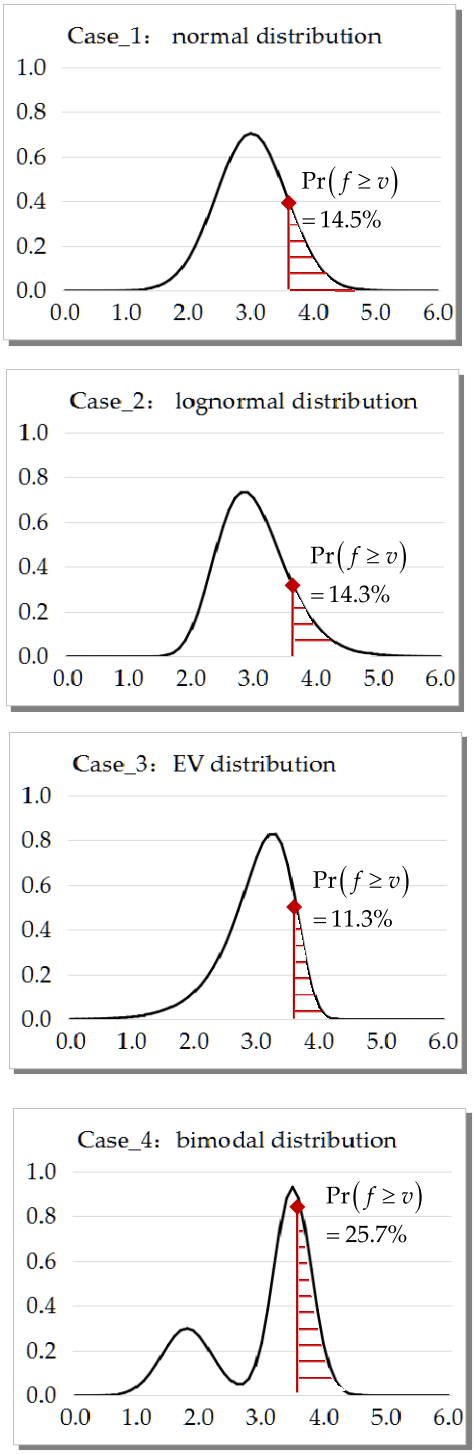

FIGURE 1. Four random responses with the same mean and variance.

respectively follow a normal distribution, a lognormal distribution, an extreme value distribution, and a bimodal distribution. The PDFs are detailed in TABLE 1. Under the mean-variance-based robustness metrics, the four cases of random responses bring the same level of quality loss. From the perspective of quality assurance in engineering, however, the quality loss of these cases is different. For a smaller-the-better problem with the accept/reject limit (ARL) of $v = 3.6$,

the failure probabilities in the four cases are 14.5%, 14.3%, 11.3%, and 25.7%, respectively. The results show that the failure probability of the fourth case is much more than that of others. Therefore, the mean-variance-based robustness metrics seem to be inappropriate in many cases involving multimodal distributions.

To address this issue, the distribution of performance response is employed directly to formulate the robust optimization model. That is, the probability of $f \geq v$ is minimized, where f denotes the performance function and v is the ARL. Note that, unless the designer has a clear picture of the engineering problem, fixing the ARL may be a problematic decision problem. Thus, v is processed into a new-added design variable. The robust optimization model for a smaller-the-better problem is formulated as

$$\begin{aligned} &\min_{\boldsymbol{d},\boldsymbol{\mu_X},v} \ v, \quad \min \ P_f \\ &\text{s.t. } P_f = \Pr\left(f\left(\boldsymbol{d},\boldsymbol{X},\boldsymbol{P}\right) \geq v\right) \leq P_f^a \\ &\quad \boldsymbol{d}^l \leq \boldsymbol{d} \leq \boldsymbol{d}^u, \ \boldsymbol{\mu_X^l} \leq \boldsymbol{\mu_X} \leq \boldsymbol{\mu_X^u} \end{aligned} \tag{4}$$

where d is the n_d-dimensional deterministic design vector; X is the n_X-dimensional random design vector; P is the n_P-dimensional random parameter vector; the superscripts of l, u represent the value range of a design variable; $\boldsymbol{\mu}$ represents the mean vector of random vector; Pr represents probability calculation; and P_f^a denotes the allowable reject ratio which is usually given according to the engineering experience or quality standards. Note that, the problems of larger-the-better $\left(f^L\right)$ and normal-the-best $\left(f^N\right)$ can be converted into the smaller-the-better problem, such as $f = -f^L$ and $f = \left(f^N\right)^2$.

The proposed model can be viewed as an extension of classical robust optimization. Minimizing v is to improve the product performance, and minimizing $\Pr\left(f \geq v\right)$ is to reduce the quality loss caused by uncertainties. Due to considering the distribution of f instead of its mean and variance, the proposed robustness metric can directly reflect the quality loss and results in higher accuracy. Also, it should be pointed out that determining $\Pr\left(f \geq v\right)$ analytically will almost always be excluded except for some explicit-function-based problems. Engineering problems are usually based on the time-consuming simulation model, such as finite element model [32] or multi-body dynamics model [33]. Calculating $\Pr\left(f \geq v\right)$ numerically will be computationally expensive because of a large number of simulation model calculations. Since $\Pr\left(f \geq v\right)$ is to be optimized, the probability calculation is in the inner loop of the optimization process. That is, the overall computational complexity increases considerably in the robust optimization.

IV. THE PROPOSED ALGORITHM

A decoupling algorithm is developed to solve the robust optimization as Equation (4) to improve the efficiency. Its basic idea is to decouple the probability calculation from the inner loop of the optimization and convert the robust optimization into a sequence iteration process. The probability calculation and the design optimization are performed alternately until convergence. The proposed algorithms are given below to illustrate in details.

A. PROBABILITY CALCULATION

During the optimization process, the probability calculation is used to evaluate the performance robustness at each design point. At a certain design point $(\boldsymbol{d}, \boldsymbol{\mu_X}, v)$, $\Pr\left(f \geq v\right)$ can be written in the following integral form:

$$\Pr\left(f \geq v\right) = \int_v^{+\infty} \rho_f\left(f\left(\boldsymbol{Z}\right)\right) \mathrm{d}f \tag{5}$$

where $\boldsymbol{Z} = (\boldsymbol{X}, \boldsymbol{P})$, and ρ_f represents the PDF of the performance response. Equation (5) is a multidimensional integral problem which can hardly be solved analytically unless the analytical formula of ρ_f is obtained. Monte-Carlo simulation [34] usually is computationally expensive to solve it numerically due to the time-consuming calculations of the performance function. Although the first-order methods (e.g., FOSM [35]) are efficient, the accuracy of them may be insufficient when the input certainties involving multimodal distributions.

To enhance the efficiency and accuracy, the second-order higher moment (SOHM) method is proposed to determine $\Pr\left(f \geq v\right)$. Firstly, the central moments are obtained according to the PDF of each input random variable, which can be expressed as

$$\begin{aligned} M^j\left(Z_i\right) &= E\left(Z_i - \mu_{Z_i}\right)^j \\ &= \int_{-\infty}^{+\infty} \left(Z_i - \mu_{Z_i}\right)^j \rho_Z^i\left(Z_i\right) dZ_i \end{aligned} \tag{6}$$

where is the j-th order moment of the random variable Z_i, E represents mean calculation, ρ_Z^i denotes the PDF of Z_i which has been formulated by the GMM illustrated in Section 1, and the mean μ_{Z_i} can be calculated as

$$\mu_{Z_i} = E\left(Z_i\right) = \int_{-\infty}^{+\infty} Z_i \rho_Z^i\left(Z_i\right) dZ_i \tag{7}$$

Secondly, the second-order Taylor approximation for $f\left(\boldsymbol{Z}\right)$ is established at the mean point of $\boldsymbol{\mu_Z}$:

$$\begin{aligned} f \approx H =& f\left(\boldsymbol{\mu_Z}\right) + \left(\boldsymbol{Z} - \boldsymbol{\mu_Z}\right)^T \nabla f\left(\boldsymbol{\mu_Z}\right) \\ &+ \frac{1}{2}\left(\boldsymbol{Z} - \boldsymbol{\mu_Z}\right)^T \nabla^2 f\left(\boldsymbol{\mu_Z}\right)\left(\boldsymbol{Z} - \boldsymbol{\mu_Z}\right) \end{aligned} \tag{8}$$

For most engineering problems, the uncertainty for a variable behaves as the small perturbation around its nominal value. Thus, the second-order approximation method [35] generally can guarantee accuracy. Thirdly, the central moments of the performance response are calculated based on the moments of Z_i. Combining Equation (8), the first-fourth order moments of $f\left(\boldsymbol{Z}\right)$ can be calculated

analytically [36]:

$$\begin{aligned}
M^1(f) &= f(\boldsymbol{\mu}_{\boldsymbol{Z}}) + \frac{1}{2}\sum_{i=1}^{n_Z}\frac{\partial^2 f(\boldsymbol{\mu}_{\boldsymbol{Z}})}{\partial Z_i^2}M^2(Z_i)\\
M^2(f) &= \sum_{i=1}^{n_Z}\left(\frac{\partial f(\boldsymbol{\mu}_{\boldsymbol{Z}})}{\partial Z_i}\right)^2 M^2(Z_i)\\
&\quad + \sum_{i=1}^{n_Z}\frac{\partial f(\boldsymbol{\mu}_{\boldsymbol{Z}})}{\partial Z_i}\frac{\partial^2 f(\boldsymbol{\mu}_{\boldsymbol{Z}})}{\partial Z_i^2}M^3(Z_i)\\
&\quad + \frac{1}{4}\sum_{i=1}^{n_Z}\left(\frac{\partial^2 f(\boldsymbol{\mu}_{\boldsymbol{Z}})}{\partial Z_i^2}\right)^2\left(M^4(Z_i) - 3\left(M^2(Z_i)\right)^2\right)\\
&\quad + \frac{1}{2}\sum_{i=1}^{n_Z}\sum_{j=1}^{n_Z}\left(\frac{\partial^2 f(\boldsymbol{\mu}_{\boldsymbol{Z}})}{\partial Z_i\partial Z_j}\right)^2 M^2(Z_i)M^2(Z_j) \qquad (9)\\
M^3(f) &= \sum_{i=1}^{n_Z}\left(\frac{\partial f(\boldsymbol{\mu}_{\boldsymbol{Z}})}{\partial Z_i}\right)^3 M^3(Z_i)\\
&\quad + \frac{3}{2}\sum_{i=1}^{n_Z}\left(\frac{\partial^2 f(\boldsymbol{\mu}_{\boldsymbol{Z}})}{\partial Z_i^2}\right)^2\frac{\partial^2 f(\boldsymbol{\mu}_{\boldsymbol{Z}})}{\partial Z_i^2}\\
&\quad \times\left(M^4(Z_i) - 3\left(M^2(Z_i)\right)^2\right)\\
&\quad + 3\sum_{i=1}^{n_Z}\sum_{j=1}^{n_Z}\frac{\partial f(\boldsymbol{\mu}_{\boldsymbol{Z}})}{\partial Z_i}\frac{\partial f(\boldsymbol{\mu}_{\boldsymbol{Z}})}{\partial Z_j}\frac{\partial^2 f(\boldsymbol{\mu}_{\boldsymbol{Z}})}{\partial Z_i\partial Z_j}M^2(Z_i)\\
&\quad \times\left(M^2(Z_j)\right)^2\\
M^4(f) &= \sum_{i=1}^{n_Z}\left(\frac{\partial f(\boldsymbol{\mu}_{\boldsymbol{Z}})}{\partial Z_i}\right)^4\left(M^4(Z_i) - 3\left(M^2(Z_i)\right)^2\right)\\
&\quad + 3\sum_{i=1}^{n_Z}\sum_{j=1}^{n_Z}\left(\frac{\partial f(\boldsymbol{\mu}_{\boldsymbol{Z}})}{\partial Z_i}\right)^2\left(\frac{\partial f(\boldsymbol{\mu}_{\boldsymbol{Z}})}{\partial Z_j}\right)^2\\
&\quad \times M^2(Z_i)M^2(Z_j)
\end{aligned}$$

The higher order moments can be obtained by the recursive formula as

$$M^j = -\frac{j}{1+(j+1)c_2}\left(c_0 M^{j-2} + c_1 M^{j-1}\right) \qquad (10)$$

where

$$\begin{aligned}
c_0 &= \frac{1}{A}M^2\left(4M^2M^4 - 3\left(M^3\right)^2\right)\\
c_1 &= \frac{1}{A}M^3\left(3\left(M^2\right)^2 - M^4\right)\\
c_2 &= \frac{1}{A}\left(2M^2M^4 - 3\left(M^3\right)^2 - 6\left(M^2\right)^3\right)\\
A &= 18\left(M^2\right)^3 - 10M^2M^4 + 12\left(M^3\right)^2 \qquad (11)
\end{aligned}$$

Here, for convenience of expression, $M^j(f)$ is abbreviated as M^j.

After determining $M^j(f), j = 1, 2, \ldots, n_m$, the maximum entropy method [37] is used to formulate the PDF of the response performance. The mathematical models can be written as

$$\begin{aligned}
&\max\ S = -c\cdot\int \rho_f \log\left(\rho_f\right)\mathrm{d}f\\
&\text{s.t.}\ \int_{-\infty}^{+\infty}\left(f-\mu_f\right)^j\rho_f df = M^j(f), \quad j = 1, 2, \ldots, n_m
\end{aligned} \qquad (12)$$

where ρ_f represents the PDF of f, c is a positive constant, and S denotes the Shannon entropy of ρ_f. The mathematical structure of ρ_f is established by Lagrangian multipliers:

$$\rho_f = \exp\left(-\sum_{i=0}^{n_\lambda}\lambda_i f^i\right) \qquad (13)$$

where $\lambda_i, i = 1, 2, \ldots, n_\lambda$ are the undetermined distribution parameters.

From the above analysis, it can be observed that Equation (12) is a multivariate optimization problem with n_m number of constraints, in which the entropy is optimized about λ_i. However, determining n_m remains an unresolved but essential issue. On the one hand, more high-order moments are required for modeling the multimodal characteristic of the performance response. On the other hand, including more constraints, mean higher complexity for solving Equation (12), which will lead to non-convergence. Fortunately, Equation (11) does not involve performance function evaluation. That is, the computational cost can be ignored. The exhaustive search strategy is a natural choice. In this way, Equation (12) is solved on the given n_m with starting from four, one by one until the optimum of entropy achieves convergence. By substituting the analytic expression of ρ_f into Equation (5), $\Pr(f \geq v)$ can be eventually determined.

B. DECOUPLING STRATEGY

In the previous section, each of the probability calculation is realized efficiently. However, it is still the inner loop of the robust optimization, and a large number of probability calculations is required. To reduce the solving complexity, the weight factor of w is used to aggregate the two objectives in a single objective, and Equation (4) can be rewritten as

$$\begin{aligned}
&\min_{\boldsymbol{\mu}_{\boldsymbol{X}}, v}\ (1-w)\cdot\frac{v}{\mu_f^{(0)}} + w\cdot\frac{P_f}{P_f^a}\\
&\text{s.t.}\ P_f = \Pr(f(\boldsymbol{d}, \boldsymbol{X}, \boldsymbol{P}) \geq v) \leq P_f^a\\
&\quad \boldsymbol{\mu}_{\boldsymbol{X}}^l \leq \boldsymbol{\mu}_{\boldsymbol{X}} \leq \boldsymbol{\mu}_{\boldsymbol{X}}^u
\end{aligned} \qquad (14)$$

where $1\Big/\mu_f^{(0)}$ and $1\Big/P_f^a$ are used as the normalizing factors to eliminate the difference in magnitude between the two objective function values, and $\mu_f^{(0)} = f\left(\boldsymbol{\mu}_{\boldsymbol{X}}^{(0)}, \boldsymbol{\mu}_{\boldsymbol{P}}\right)$ is the performance function value at the initial point. For ease of representation, the deterministic design variables are treated as the random variable with zero-variance and are collected into $\boldsymbol{X}$.

To further improve efficiency, a decoupling strategy is developed to convert the original double-loop process into

a sequence iterative one with conducting the probabilistic calculation and the design optimization alternately. For fast convergence, the initial point $\boldsymbol{\mu}_{\boldsymbol{X}}^{(0)}$ is obtained by solving the deterministic optimization problem as

$$\begin{aligned} &\min_{\boldsymbol{\mu}_{\boldsymbol{X}}} f\left(\boldsymbol{\mu}_{\boldsymbol{X}}, \boldsymbol{\mu}_{\boldsymbol{P}}\right) \\ &\text{s.t. } \boldsymbol{\mu}_{\boldsymbol{X}}^{l} \leq \boldsymbol{\mu}_{\boldsymbol{X}} \leq \boldsymbol{\mu}_{\boldsymbol{X}}^{u} \end{aligned} \tag{15}$$

where the uncertainties in $\boldsymbol{X}, \boldsymbol{P}$ being neglected. Then, the first iteration begins, i.e., $k = 1$. Firstly, the optimization problem without performance function evaluation is formulated as

$$\begin{aligned} &\min_{\boldsymbol{\mu}_{\boldsymbol{X}}, v} \ (1-w) \cdot \frac{v}{\mu_f^{(0)}} + w \cdot \frac{P_f}{P_f^a} \\ &\text{s.t. } P_f = \Pr\left(H^{(k)} \geq v\right) + e^{(k-1)} \leq P_f^a \\ &\quad \boldsymbol{\mu}_{\boldsymbol{X}}^{l} \leq \boldsymbol{\mu}_{\boldsymbol{X}} \leq \boldsymbol{\mu}_{\boldsymbol{X}}^{u} \end{aligned} \tag{16}$$

where $H^{(k)}$ is the updated second-order Taylor approximation, as Equation (8), for the performance function at $\left(\boldsymbol{\mu}_{\boldsymbol{X}}^{(k-1)}, \boldsymbol{\mu}_{\boldsymbol{P}}\right)$. Equation (16) is modified based on Equation (14), which is solved to obtain the updated solution $\boldsymbol{\mu}_{\boldsymbol{X}}^{(k)}, v^{(k)}$, and $P_f^{(k)} = \Pr\left(H^{(k)} \geq v^{(k)}\right)$. Because of the approximation of $H^{(k)}$ is employed, an error is inevitably introduced into the probability calculation. In Equation (16), $e^{(k)}$ is used to correct $P_f^{(k)}$, namely $e^{(k)} = \hat{P}_f^{(k)} - P_f^{(k)}$ where $\hat{P}_f^{(k)}$ denotes the relatively accurate result of probability calculation.

Here, the proposed SOHM is still being used for the calculation of $\hat{P}_f^{(k)}$, but the accuracy needs to be further improved. One of the ways is to optimize the position of the Taylor expansion point in Equation (8). For the current point of $\boldsymbol{\mu}_{\boldsymbol{X}}^{(k)}$, the most probability point (MPP) is the point with the most joint PDF on the limit-state boundary of $f = v^{(k)}$. Compared to other points on the boundary, the Taylor approximation at the MPP can achieve the minimal error of reliability analysis [38]. The searching process of the MPP can be formulated as

$$\begin{aligned} &\max_{\boldsymbol{Z}} \ \rho_{\boldsymbol{Z}}\left(\boldsymbol{Z} | \boldsymbol{\mu}_{\boldsymbol{X}}^{(k)}\right) \\ &\text{s.t. } f\left(\boldsymbol{Z}\right) = v^{(k)} \end{aligned} \tag{17}$$

where $\boldsymbol{Z} = (\boldsymbol{X}, \boldsymbol{P})$. The MPP of $\boldsymbol{Z}_{MPP}^{(k)}$ can be obtained by solving Equation (17). Next, $\hat{P}_f^{(k)}$ is obtained by the SOHM method based on the $\boldsymbol{Z}_{MPP}^{(k)}$.

Due to the lack of information from the previous step, $e^{(0)} = 0$ is set in the first iteration step ($k = 1$). The design optimization as Equation (16) and the uncertainty analysis as Equation (17) is performed alternatively until the following convergence criteria are satisfied:

$$\begin{cases} \left| \dfrac{Pf^{(k)} - Pf^{(k-1)}}{Pf_j^{(k)}} \right| \leq \varepsilon_r \\ \left| \dfrac{e^{(k)}}{v_j^{(k)}} \right| \leq \varepsilon_r \end{cases} \tag{18}$$

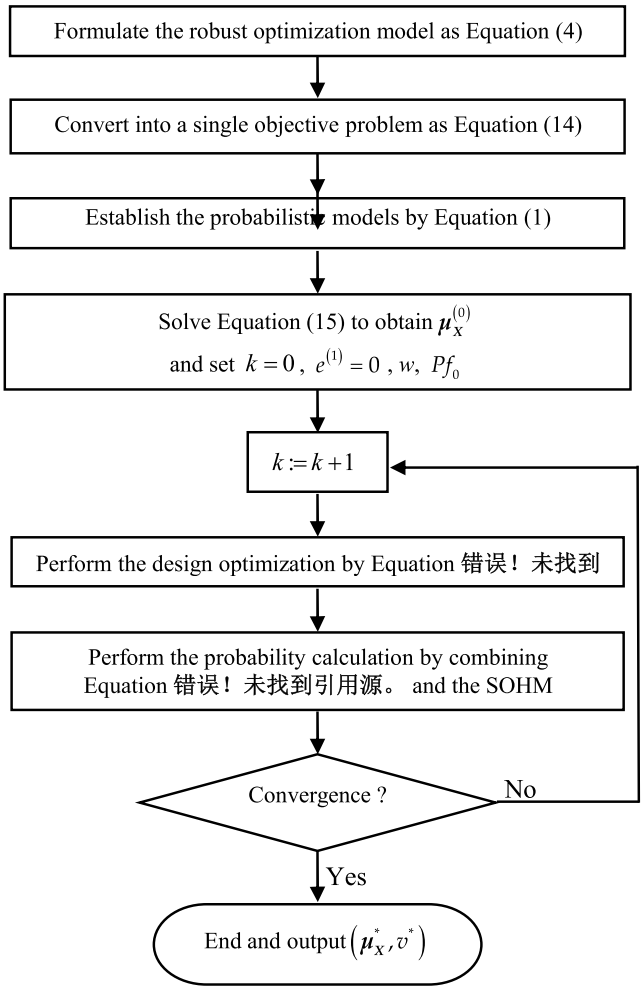

FIGURE 2. The flowchart of the proposed method.

The flowchart of the proposed method is summarized in FIGURE 2.

V. APPLICATION DISCUSSION

The purpose of this study is to provide a potential tool of the robust optimization for similar products or systems. In this section, the engineering practicability of the proposed method is discussed through three applications: a sweat-rate sensor, a piezoelectric sensor, and an image sensing module. The features of the proposed method are investigated in terms of efficiency and accuracy by accounting the performance function evaluations and comparing the reference solution. The reference solution is obtained by the double-loop method (DLM), where the sequential quadratic programming [39] is employed for the design optimization in the outer loop, and Monte-Carlo simulation [34] is used for the probabilistic calculation in the inner loop.

A. A SWEAT-RATE SENSOR

Sweat-rate sensors [40] can monitor the human thermal status and has been required for many wearable devices to check the user's physiological conditions. FIGURE 3 shows the

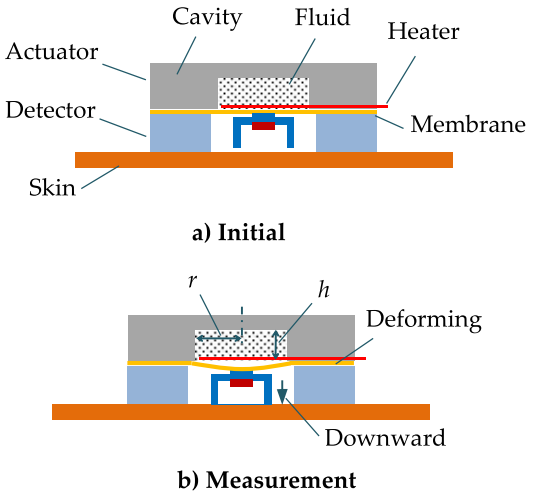

FIGURE 3. The structure of a sweat-rate sensor.

structure of a wearable sweat rate sensor. It is composed of a sweat rate detector and a thermopneumatic actuator. In the actuator, the heater controls the temperature of the expansion fluid. The temperature-dependent vapor pressure of the expansion fluid deforms the membrane, thus moving the detector upward or downward directions. When the detector is close to the skin, it starts measuring the sweat rate. After each measurement, the detector is separated from the skin to ventilate the collected humidity.

The time response of each measurement is generally considered as the critical performance for the sweat-rate sensors. It is formulated as [40]

$$t = m \cdot C \cdot R_t \cdot \log\left(1 - \frac{(T_b - T_a) \cdot R}{V^2 \cdot R_t}\right) \tag{19}$$

where m, C and T_b denote the mass, heat capacity and boiling temperature of the expansion fluid, R is the thermal resistance between the expansion fluid and the surrounding air, T_a denotes the surrounding temperature, and R, V represent the electrical resistance and input voltage of the heater. Here, m can be written as $m = \rho \cdot v$ where the volume $v = \pi \cdot r^2 \cdot h$ and the density $\rho = 1.68 \times 10^{-3}\mathrm{g}/\mathrm{mm}^3$. The material properties of C, T_b are the constants: $C = 1.05 \times 10^3 \mathrm{J}/(\mathrm{g} \cdot^\circ \mathrm{C})$, $T_b = 56\ ^\circ\mathrm{C}$. The height of the fluid cavity is given as the fixed value: $h = 1$ mm. $T_a = 25\ ^\circ\mathrm{C}$ refers to the standard test environment in the standard test. R_E, V and r are the design variables. Due to the requirement of compact sizes, the input power is limited. The design variable V and the parameter R are uncertain and are treated as random variables. Their probability distributions are shown in FIGURE 4. After giving the weight factor of $w = 0.5$ for the two objectives in Equation (4), the robust optimization problem is modeled as

$$\begin{aligned} \min_{r,R_E,\mu_V,v_t} \quad & (1-w) \cdot \frac{v}{t^{(0)}} + w \cdot \frac{P_f}{P_f^a} \\ \text{s.t. } & P_f = \Pr\left(t\left(r, R_E, V, R\right) \geq v\right) \geq P_f^a = 95\% \\ & 5\ \text{mm} \leq r \leq 10\ \text{mm} \\ & 30\ \Omega \leq R_E \leq 90\ \Omega \\ & 3\ \text{V} \leq \mu_V \leq 12\text{V} \end{aligned} \tag{20}$$

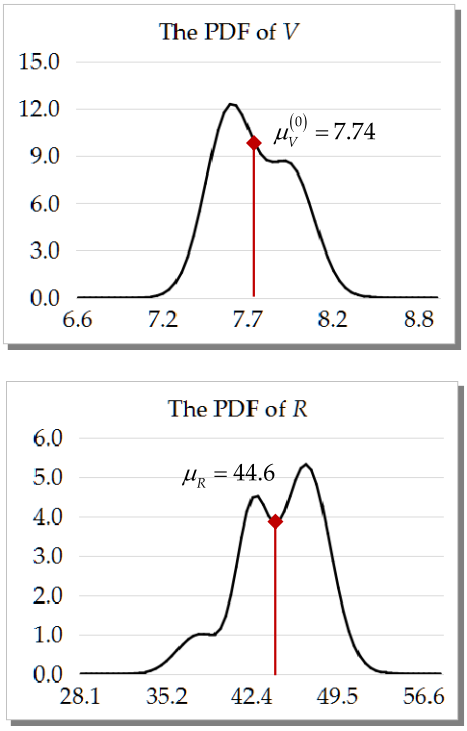

FIGURE 4. The random distribution of V and R_t.

Next, the proposed method is applied to solve Equation (20). The random variables of V, R are described as the multimodal distributions through Equation (1) and are expressed as

$$\begin{aligned} \rho_V &= 0.6 \cdot \varphi\left(V \,|0.98 \cdot \mu_V, 0.28\right) \\ &\quad + 0.4 \cdot \varphi\left(V \,|1.03 \cdot \mu_V, 0.28\right) \\ \rho_R &= 0.1 \cdot \varphi\left(R \,|37.91, 1.78\right) \\ &\quad + 0.3 \cdot \varphi\left(R \,|42.37, 1.34\right) \\ &\quad + 0.6 \cdot \varphi\left(R \,|46.83, 2.01\right) \end{aligned} \tag{21}$$

Through combined Equation (7) and (21), $\mu_R = 44.6\ ^\circ\mathrm{C}/\mathrm{W}$ is obtained. The initial point $\left(r^{(0)}, R_E^{(0)}, \mu_V^{(0)}\right) = (7.07\ \text{mm},\ 60.0\ \Omega,\ 7.74\ \text{V})$ is obtained by solving the deterministic optimization: $\min_{r,R_E,\mu_V} t\left(r, R_E, \mu_V, \mu_R\right)$. Correspondingly, $t^{(0)} = t\left(r^{(0)}, R_E^{(0)}, \mu_V^{(0)}, \mu_R\right) = 12.8\text{S}$ can be determined. Then, the first iteration step starts with setting $k = 1$ and $e^{(0)} = 0$. The second-order Taylor approximation $H^{(k)}$ is established for the performance function $t\left(r, R_E, V, R\right)$ at the point $\left(r^{(0)}, R_E^{(0)}, V^{(0)}, \mu_R\right)$. The design optimization as Equation (16) is performed to obtain the updated solution, i.e., $\left(r^{(k)}, R_E^{(k)}, \mu_V^{(k)}\right) = (7.46\ \text{mm},\ 65.6\ \Omega,\ 8.54\ \text{V})$, $v^{(k)} = 17.3$ S, and $Pf^{(k)} = 0.77\%$. To correct the error introduced by $H^{(k)}$, the position of the Taylor expansion point is optimized to the MPP, which is obtained by solving the following optimization problem:

$$\begin{aligned} \max_{V,R} \quad & \rho_{\mathbf{Z}}\left(\mathbf{Z} | \mu_V^{(k)}\right) \\ \text{s.t. } & f\left(V, R | r^{(k)}, R_E^{(k)}, \mu_V^{(k)}\right) = v^{(k)} \end{aligned} \tag{22}$$

TABLE 2. The results of the sweat-rate sensor problem.

Solutions		Mean response (S) μ_t	ARL (S) v	Probability (%) $\Pr(t \geq v)$
Solution of proposed method	1st iteration	13.7	17.3	0.77
	2nd iteration	13.2	16.3	0.52
	3rd iteration	13.1	16.3	0.59
	4th iteration	13.1	16.4	0.61
Reference solution of DLM		13.0	16.2	0.59

Then, $\hat{P}_f^{(k)}$ is calculated by using the SOHM method, and $e^{(k)} = \hat{P}_f^{(k)} - P_f^{(k)} = 1.12\%$ can be obtained. It provides the necessary information to formulate the design optimization at the next iteration step ($k = 2$):

$$\begin{aligned} &\min_{\boldsymbol{\mu}_X, v} \ (1-w)\cdot\frac{v}{\mu_f^{(0)}} + w\cdot\frac{P_f}{P_f^a} \\ &\text{s.t. } P_f = \Pr\left(t\left(r, R_E, V, R\right) \geq v\right) + e^{(k-1)} \leq P_f^a \\ &\quad 5 \text{ mm} \leq r \leq 10 \text{ mm} \\ &\quad 30\ \Omega \leq R_E \leq 90\ \Omega \\ &\quad 3 \text{ V} \leq \mu_V \leq 12\text{V} \end{aligned} \tag{23}$$

After four iteration steps, the solving process achieves convergence, and the performance function is calculated 321 times. All results are listed in TABLE 2. For this application, the proposed method exhibits excellent comprehensive performance in terms of convergence and efficiency. In terms of accuracy, the solutions of the proposed method are very close to the reference solutions, and the differences at the mean response and the ARL are 0.7% and 1.3%, respectively. Furthermore, the random distributions of $t\ (V, R)$ at the optimal solution and the initial solution are shown in FIGURE 5. The performance response at the two solutions presents the multimodal characteristic with the same number ($n_m = 8$) of peaks in their PDFs. It indicates, n_m only needs to be determined at the initial solution, and the result can directly be used during the subsequent solving process.

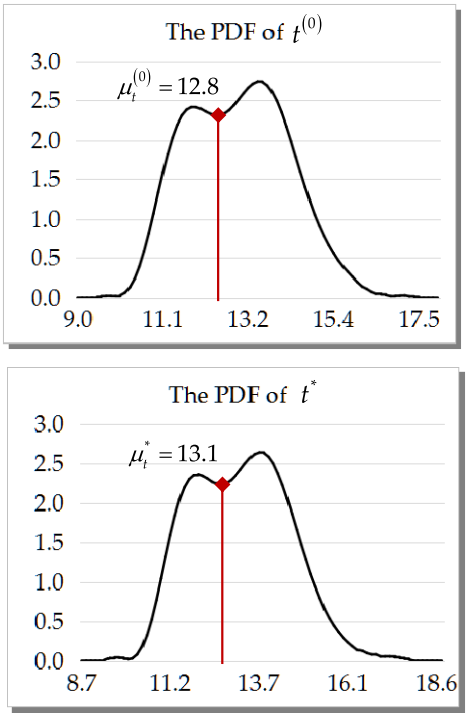

FIGURE 5. The random distributions of the performance response.

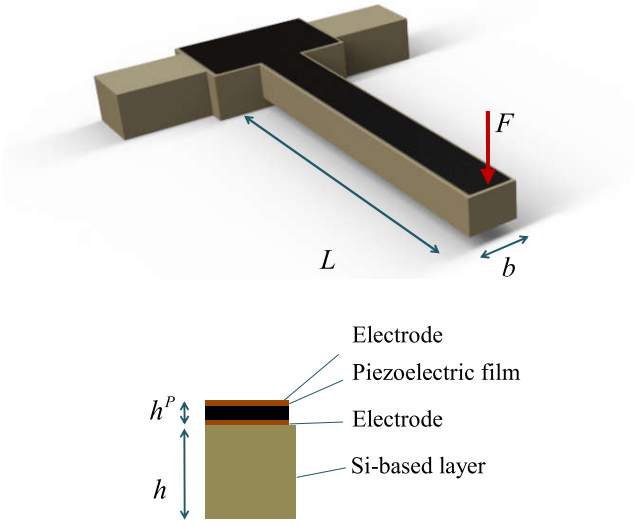

FIGURE 6. A piezoelectric cantilever beam.

B. A PIEZOELECTRIC MICRO-FORCE SENSOR

A piezoelectric sensor has many advantages, including a reliable structure, fast response, and pure driving circuits. It has been extensively applied in the fields of precision positioning, ultrasonic devices, micro-force measurement, etc. The piezoelectric bimorph beam, as in FIGURE 6, is a typical sensing structure of the piezoelectric sensor. It is composed of a piezoelectric film, a silicon-based layer, and two electrodes. The force at the free end bends the beam and then causes the piezoelectric film output polarization charges. Finally, the charges are converted into a voltage signal. The process can be formulated as [42]

$$U = \frac{3\cdot d_{31}^P \cdot S_{11}^{Si} \cdot S_{11}^P \cdot h \cdot h^P \cdot \left(h + h^P\right) \cdot L \cdot F}{K \cdot \varepsilon_{33}^P \cdot w} \tag{24}$$

where

$$\begin{aligned} K = {} & 4\cdot S_{11}^{Si}\cdot S_{11}^P \cdot h \cdot \left(h^P\right)^3 + 4\cdot S_{11}^{Si}\cdot S_{11}^P \cdot h^3 \cdot h^P \\ & + \left(S_{11}^P\right)^2 \cdot h^4 + \left(S_{11}^{Si}\right)^2 \cdot \left(h^P\right)^4 \\ & + 4\cdot S_{11}^{Si}\cdot S_{11}^P \cdot \left(S_{11}^{Si}\right)^2 \cdot \left(h^P\right)^2 \end{aligned} \tag{25}$$

where F is the concentration force; L, w represent the length and width of the beam; h, h^P denote the thickness of the silicon-base layer and piezoelectric film; S_{11}^{Si},S_{11}^{P} are the compliance coefficient of the silicon-based layer and piezoelectric film; and d_{31}^P, ε_{33}^P is the piezoelectric coefficient and dielectric constant of the piezoelectric film. The constants in Equation (24) include $h^P = 5 \times 10^{-4}$ mm, $S_{11}^P = 18.97 \times 10^{-12}\text{m}^2/\text{N}$, and $S_{11}^{Si} = 7.70 \times 10^{-12}\text{m}^2/\text{N}$. Here, the material parameter of d_{31}^P ε_{33}^P are treated as random variables. Their PDFs can be obtained using Equation (1) based on statistical data in practical engineering, while in this example they are directly given as

$$\begin{aligned}\rho_d &= 0.30 \cdot \varphi\left(d_{31}^P \,|1.62, 0.072\right) \\ &\quad + 0.70 \cdot \varphi\left(d_{31}^P \,|1.88, 0.090\right) \\ \rho_\varepsilon &= 0.65 \cdot \varphi\left(\varepsilon_{33}^P \,|1.70, 0.080\right) \\ &\quad + 0.35 \cdot \varphi\left(\varepsilon_{33}^P \,|1.41, 0.080\right)\end{aligned} \tag{26}$$

Generally, sensitivity is the fundamental performance of the piezoelectric sensor, which is dependent on the output voltage under a particular load. Thus, U is viewed as the objective function. The design variables are L, b, and h. The constraints of the shape, stiffness, and strength are considered, which are expressed as $\eta = b/h \geq 0.83$, $\delta \leq 2.5$ μm, and $\sigma \leq 32.0$ MPa. Here, δ denotes the displacement at the free end of the beam, and σ denotes the maximum stress of the beam. δ and σ can be written as [42]

$$\begin{aligned}\sigma &= \frac{6 \cdot F \cdot L \cdot S_{11}^{Si} \cdot \left(S_{11}^P \cdot h + S_{11}^{Si} \cdot h^P\right) \cdot \left(h + h^P\right)}{K \cdot b} \\ \delta &= \frac{4 \cdot F \cdot L^3 \cdot S_{11}^{Si} \cdot S_{11}^P \cdot \left(S_{11}^P \cdot h + S_{11}^{Si} \cdot h^P\right)}{K \cdot b}\end{aligned} \tag{27}$$

Note that this is a larger-the-better problem. After a simple conversion, the robust optimization is formulated as

$$\begin{aligned}\min_{L,b,h,v} \quad & -(1-w) \cdot \frac{v}{\mu_U^{(0)}} + w \cdot \frac{P_f}{P_f^a} \\ \text{s.t. } & P_f = \Pr\left(U\left(L, b, h, d_{31}^P, \varepsilon_{33}^P\right) \leq v\right) \leq P_f^a \\ & b/h \leq 0.83, \ \delta(L, b, h) \leq 2.5\mu m, \\ & \sigma(L, b, h) \leq 32.0\text{MPa} \\ & 0.40\text{mm} \leq L \leq 1.20\text{mm} \\ & 0.06\text{mm} \leq b \leq 0.10\text{mm} \\ & 0.04\text{mm} \leq h \leq 0.10\text{mm}\end{aligned} \tag{28}$$

To demonstrate the practicality of the proposed method, the three cases with different w are considered: 0.2, 0.5, 0.8. The higher w indicates that the designer pays more attention to the performance robustness. The proposed methods and the DLM are used to solve Equation (28) in these cases. The solving processes start with the same initial point of (0.788 mm, 0.081mm, 0.068mm) calculated by the deterministic optimization: $\min_{L,w,h} \ U$. Moreover, the results are shown in TABLE 3. It can be observed that the results of the two methods in each case are very close, which verifies the accuracy of the proposed method. The results also show, the mean response decreases as the weight of robustness increases. $\mu_U^* = 36.27$ mV in Case 1 is 20.9% more than $\mu_U^* = 28.68$ mV in Case 3. That is, if a higher weight factor is defined for the robustness, the optimal design will exhibit relatively poor performance. In addition, the solutions under various weights can help designers create a relatively clear picture of the design problem without excessive computational cost. In this application, the three solving processes calculate the performance function for 915 times. This provides an alternative to directly call time-consuming simulation models for improving the accuracy of robust optimization.

TABLE 3. The results of the micro-force senor problem.

Results	DLM		The proposed method			
	DV (mm)	MRV (mV)	DV (mm)	MRV (mV)	ARL (mV)	Probability (%)
	L, b, h	μ_U	L, b, h	μ_U	v	Pr
Case 1: $w = 0.2$	0.758, 0.089, 0.063	36.78	0.756, 0.090, 0.063	36.27	32.86	0.51
Case 2: $w = 0.5$	0.782, 0.094, 0.069	29.97	0.789, 0.095, 0.070	29.05	26.32	0.43
Case 3: $w = 0.8$	0.778, 0.095, 0.069	29.19	0.776, 0.095, 0.070	28.68	25.93	0.38

DV: Design Variable, MRV: Mean Response Value

C. AN IMAGE SENSING MODULE

Recently, low light imaging [43] is being researched intensively. The applications of ultra-low-noise image sensing modules expand to security, biomedicine, and exploration. In the image sensing module as FIGURE 7, the ultra-low-noise image sensor and other components are assembled on the printed circuit board (PCB). Due to the mismatch in the thermal expansion coefficient of the various materials, thermal deformation occurs on the PCB under the effects of self-heating and changing ambient temperature. This leads to a loss of image quality. Especially for the large format sensors, its performance is more sensitive to the deformation.

In order to analyze the thermal deformation of the module under the changing temperature (20°C $\sim$ 45°C), the finite element model (FEM) is created as shown in FIGURE 8, in which the structural size of the PCB is 42mm $\times$ 42mm $\times$ 1.6mm, and the power dissipation of the codec chip and the converter is given as $\mu_{P_1} = 1.5$W, $\mu_{P_1} = 0.3$W according to the test data. It can be observed that the deformation appears on the sensor die, and the peak-peak value (PPV) of the displacement response is about 0.109 mm. To reduce the image quality loss of the module, the PPV needs to be optimized. Adjusting the relative position of the module-fixed points is a low-cost way to reduce the PPV, and thus, the positions

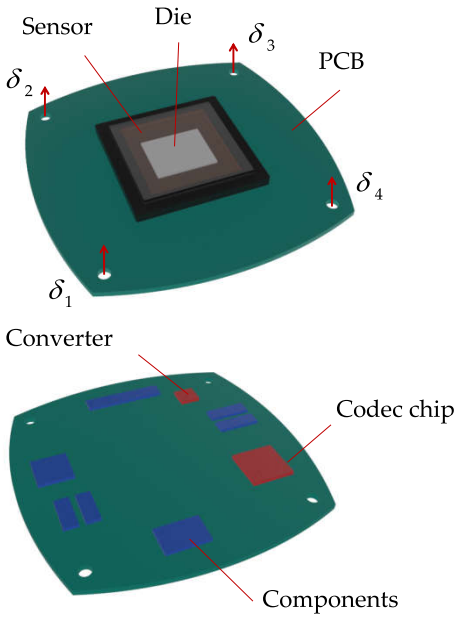

FIGURE 7. The image sensing module with an ultra-low-noise sensor.

$\boldsymbol{\delta} = (\delta_1, \delta_2, \delta_3, \delta_4)$ are set as the design variables. Given that manufacturing errors are unavoidable, each component of $\boldsymbol{\delta}$ is treated as the random variable with the same variance of $\sigma_i^2 = 0.0003\text{mm}, i = 1, 2, 3, 4$. The robust optimization is formulated as

$$\begin{aligned} &\min_{\boldsymbol{\delta}, v} \ (1-w)\cdot\frac{v}{\mu_{PPV}^{(0)}} + w\cdot\frac{P_f}{Pf_0} \\ &s.t.\ P_f = \Pr\left(PPV\left(\boldsymbol{\delta}\right) \le v\right) \le Pf_0 \end{aligned} \tag{29}$$

where $\mu_{PPV}^{(0)} = PPV\left(\boldsymbol{\mu}_{\boldsymbol{\delta}}^{(0)}\right)$, $Pf_0 = 95\%$, and $w = 0.5$. As mentioned above, the performance function of PPV is implicit and based on the time-consuming FEM, which consists of 30,108 eight-node thermally coupled hexahedron elements. The computational time for solving the FEM is about 0.3 hours if using a computer with the i7-4710HQ CPU and 8 G of RAM. To realize the parameterization and reduce the computational cost of obtaining reference solutions, a second-order polynomial response surface is created for the performance function by sampling 200 times on the FEM.

$$\begin{aligned} PPV = {} & 0.109 - 0.718\delta_1 + 1.023\delta_2 + 0.286\delta_3 \\ & - 0.634\delta_4 + 3.756\delta_1^2 + 3.611\delta_2^2 + 2.328\delta_3^2 \\ & + 2.254\delta_4^2 - 3.035\delta_1\delta_2 - 6.312\delta_1\delta_3 + 1.542\delta_1\delta_4 \\ & - 1.857\delta_2\delta_3 - 4.938\delta_2\delta_4 + 0.741\delta_3\delta_4 \end{aligned} \tag{30}$$

To investigate the necessity of considering multimodal distributions for the robust optimization, three cases for solving Equation (29) are considered. Each variable of $\boldsymbol{\delta}$ follows: Case_1) the normal distribution, Case_2) the extreme value (EV) distribution, Case_3) the bimodal distribution. Their PDFs are listed in TABLE 4. They are solved by the proposed method and the DLM. The same initial design option is selected as $\boldsymbol{\mu}_{\boldsymbol{\delta}}^{(0)} = (0\text{ mm},\ 0\text{ mm},\ 0\text{ mm},\ 0\text{ mm})$, at which

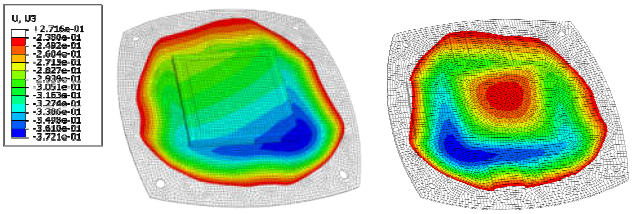

FIGURE 8. The FEM of the image-sensor-mounted PCB.

TABLE 4. The pdf of δ_i in the three cases.

Cases	PDF of δ_i with $\sigma_i^2 = 0.0003\text{mm}, i = 1,2,3,4$
Normal distribution	$\rho_\delta = \varphi\left(\delta \middle\| \mu_\delta, 0.017\right)$
EV distribution	$\rho_\delta = \frac{1}{0.013}\exp\left(-\exp\left(\frac{\delta-\left(\mu_\delta+0.007\right)}{0.013}\right)\right)$
Bimodal distribution	$\rho_\delta = 0.30\cdot\varphi\left(\delta \middle\| \mu_\delta - 0.02, 0.008\right)$ $+0.70\cdot\varphi\left(\delta_i \middle\| \mu_\delta + 0.01, 0.012\right)$

TABLE 5. The results of the image sensing module problem.

Results	DLM		The proposed method				
	DV (mm) $\boldsymbol{\mu}_{\boldsymbol{\delta}}^*$	MRV(mm) μ_{PPV}^*	DV (mm) $\boldsymbol{\mu}_{\boldsymbol{\delta}}^*$	MRV (mm) μ_{PPV}^*	ARL (mm) v^*	Pr (%) P_f	FE N_f
Case 1: Normal	-0.023, -0.101, -0.110, 0.066	0.011	-0.023, -0.101, -0.107, 0.076	0.012	0.025	2.8	298
Case 2: EV	-0.022, -0.101, -0.107, 0.071	0.011	-0.022, -0.098, -0.117, 0.074	0.010	0.022	1.5	302
Case 3: bimodal	-0.047, -0.113, -0.119, 0.055	0.002	-0.053, -0.113, -0.119, 0.053	0.002	0.020	4.1	352

$\mu_{PPV}^{(0)} = 0.109\text{mm}$. All results are listed in TABLE 5. Firstly; the results of the proposed method are almost identical with the reference solutions in each case. This indicates that the results of the proposed method are valid. In the and three cases, the values of μ_{PPV} are greatly optimized. Compared to $\mu_{PPV}^{(0)}$, they are reduced by 88.9%, 91.0%, and 98.2%, respectively, and therefore the thermal deformation of the module at $\boldsymbol{\mu}_{\boldsymbol{\delta}}^*$ is improved significantly. Secondly, the result $\left(\mu_{PPV}^*\right)$ of Case 1 is close to that of Case 2, while it is very different from that of Case 3. It shows that the multimodal distribution has a negligible effect on the optimal results for this example. Thus, it is necessary to establish accurate multimodal distributions for the input uncertain variables in the robust optimization. Thirdly, in terms of efficiency, the performance function evaluations of the three cases are 298, 302, and 352, respectively. Even if the proposed method

calls the FEM directly, $N_F = 352$, the maximum of the three cases, means the computational time of only about 100 hours. The efficiency is acceptable in practice.

VI. CONCLUSION

In engineering designs, uncertainties from various sources are inevitable; thus, the robust optimization is developed to improve the performance by minimizing the effects of uncertainties without eliminating these causes. The exiting researches focus on the problems with unimodal random variables. In real applications, however, the random variable may follow a multimodal distribution. In such cases, the classical robustness metrics based on mean and variance seem to be inappropriate. In this paper, an robust optimization model and the corresponding algorithm are proposed, which provide a potential tool for uncertain problems with multimodal distributions. The contribution of this study is summarized as follows. Firstly, the improved robust optimization model is formulated by introducing the concept of ARL to calculate the failure probability of the performance response. The probability calculation can directly capture the multimodal characteristics of the performance response. Secondly, the SOHM is presented to efficiently perform the probability calculation in the inner loop of design optimization. Thirdly, a decoupling strategy is proposed to separate the probability calculation from the design optimization and drive the two processes sequentially and alternately. The proposed method is applied to the three micromachine design problems, including a sweat-rate sensor, a piezoelectric sensor, and an image sensing module. In the applications, the proposed method exhibits excellent comprehensive performance in terms of accuracy and convergence. More importantly, this method provides an alternative to directly call time-consuming simulation models during the solving process, which can further improve the accuracy of the robust optimization. Also, the targeted engineering examples for peers to develop novel methods, which is beneficial to extend the application of robust optimization in micromachine systems. In the future, it will be our important research direction to develop efficient robust optimization methods for complex micromachine systems involving dynamic characteristics and coupled multiphysics.

REFERENCES

[1] S. S. Rao, *Engineering Optimization: Theory and Practice*, vol. 29, no. 9. Hoboken, NJ, USA: Wiley, 1997, pp. 802–803.
[2] V. B. Venkayya, "Structural optimization: A review and some recommendations," *Int. J. Numer. Methods Eng.*, vol. 13, no. 2, pp. 203–228, 2010.
[3] G. Taguchi and M. S. Phadke, "Quality engineering through design optimization," in *Quality Control, Robust Design, and the Taguchi Method*. Berlin, Germany: Springer, 1989, pp. 77–96.
[4] W. Y. Fowlkes, C. M. Creveling, and J. Derimiggio, *Engineering Methods for Robust Product Design: Using Taguchi Methods in Technology and Product Development*. Reading, MA, USA: Addison-Wesley, 1995, pp. 121–123.
[5] X. Gu, G. Sun, G. Li, L. Mao, and Q. Li, "A comparative study on multiobjective reliable and robust optimization for crashworthiness design of vehicle structure," *Struct. Multidisciplinary Optim.*, vol. 48, no. 3, pp. 669–684, 2013.
[6] W. Yao, X. Chen, W. Luo, M. van Tooren, and J. Guo, "Review of uncertainty-based multidisciplinary design optimization methods for aerospace vehicles," *Prog. Aerosp. Sci.*, vol. 47, no. 6, pp. 450–479, 2011.
[7] A. T. Nguyen, S. Reiter, and P. Rigo, "A review on simulation-based optimization methods applied to building performance analysis," *Appl. Energy*, vol. 113, pp. 1043–1058, Jan. 2014.
[8] J. Liu and G. Wen, "Continuum topology optimization considering uncertainties in load locations based on the cloud model," *Eng. Optim.*, vol. 50, no. 6, pp. 1041–1060, 2018.
[9] F. Li, J. Liu, G. Wen, and J. Rong, "Extending SORA method for reliability-based design optimization using probability and convex set mixed models," *Struct. Multidisciplinary Optim.*, vol. 59, no. 4, pp. 1163–1179, 2019.
[10] A. Tzvieli, "Possibility theory: An approach to computerized processing of uncertainty," *J. Amer. Soc. Inf. Sci.*, vol. 41, no. 2, pp. 153–154, 1990.
[11] I. Georgescu, *Possibility Theory and the Risk*. Berlin, Germany: Springer, 2012.
[12] X. Du, "Robust design optimization with bivariate quality characteristics," in *Structural and Multidisciplinary Optimization*. Hoboken, NJ, USA: Wiley, 2012.
[13] H.-G. Beyer and B. Sendhoff, "Robust optimization—A comprehensive survey," *Comput. Methods Appl. Mech. Eng.*, vol. 196, nos. 33–34, pp. 3190–3218, 2007.
[14] G.-J. Park, T.-H. Lee, K. H. Lee, and K. H. Hwang, "Robust design: An overview," *AIAA J.*, vol. 44, no. 1, pp. 181–191, 2012.
[15] V. Gabrel, C. Murat, and A. Thiele, "Recent advances in robust optimization: An overview," *Eur. J. Oper. Res.*, vol. 235, no. 3, pp. 471–483, Jun. 2014.
[16] Y. Q. Ni, X. W. Ye, and J. M. Ko, "Modeling of stress spectrum using long-term monitoring data and finite mixture distributions," *J. Eng. Mech.*, vol. 138, no. 2, pp. 175–183, 2011.
[17] R. S. Lima, A. Kucuk, and C. C. Berndt, "Bimodal distribution of mechanical properties on plasma sprayed nanostructured partially stabilized zirconia," *Mater. Sci. Eng., A*, vol. 327, no. 2, pp. 224–232, 2002.
[18] E. Mones, N. A. Araújo, T. Vicsek, and H. J. Herrmann, "Shock waves on complex networks," *Sci. Rep.*, vol. 4, May 2014, Art. no. 4949.
[19] J. He, X. Guan, and R. Jha, "Improve the accuracy of asymptotic approximation in reliability problems involving multimodal distributions," *IEEE Trans. Rel.*, vol. 65, no. 4, pp. 1724–1736, Dec. 2016.
[20] K. Dolinski, "First-order second-moment approximation in reliability of structural systems: Critical review and alternative approach," *Struct. Saf.*, vol. 1, no. 3, pp. 211–231, 1982.
[21] I. Elishakoff, S. Van Manen, and J. Arbocz, "First-order second-moment analysis of the buckling of shells with random imperfections," *AIAA J.*, vol. 25, no. 8, pp. 1113–1117, 1984.
[22] M. Hohenbichler and R. Rackwitz, "First-order concepts in system reliability," *Struct. Saf.*, vol. 1, no. 3, pp. 177–188, 1982.
[23] Y.-G. Zhao and T. Ono, "A general procedure for first/second-order reliabilitymethod (FORM/SORM)," *Struct. Saf.*, vol. 21, no. 2, pp. 95–112, 1999.
[24] Z. Hu and X. Du, "Reliability methods for bimodal distribution with first-order approximation," *J. Risk Uncertainty Eng. Syst. B, Mech. Eng.*, vol. 5, no. 1, 2018, Art. no. 011005.
[25] S. G. Walker, "A Laplace transform inversion method for probability distribution functions," *Statist. Comput.*, vol. 27, no. 2, pp. 439–448, 2017.
[26] B. Huang and X. Du, "Probabilistic uncertainty analysis by mean-value first order saddlepoint approximation," *Rel. Eng. Syst. Saf.*, vol. 93, no. 2, pp. 325–336, 2006.
[27] E. Garcia, N. Lobontiu, and Y. Nam, "Mechanics of MEMS: A review of modeling, analysis, and design," *Proc. SPIE*, vol. 5390, pp. 400–409, Jul. 2004.
[28] H. Wu, G. Cui, D. Zhang, and H. Liu, "Reliability evaluation and robust design of a sensor in an entire roller-embedded shapemeter," *Sensors*, vol. 18, no. 7, p. 1988, 2018.
[29] P. Paalanen, J. K. Kamarainen, J. Ilonen, and H. Kälviäinen, "Feature representation and discrimination based on Gaussian mixture model probability densities—Practices and algorithms," *Pattern Recognit.*, vol. 39, no. 7, pp. 1346–1358, 2006.
[30] C. Biernacki and S. Chrétien, "Degeneracy in the maximum likelihood estimation of univariate Gaussian mixtures with EM," *Statist. Probab. Lett.*, vol. 61, no. 4, pp. 373–382, 2008.
[31] A. P. Dempster, N. M. Laird, and D. B. Rubin, "Maximum likelihood from incomplete data via the *EM* algorithm," *J. Roy. Stat. Soc.*, vol. 39, pp. 1–22, Sep. 1977.

[32] H. Benaroya and M. Rehak, "Finite element methods in probabilistic structural analysis: A selective review," *Appl. Mech. Rev.*, vol. 41, no. 5, pp. 201–213, 1988.
[33] D. E. Stewart, "Rigid-body dynamics with friction and impact," *SIAM Rev.*, vol. 42, no. 1, pp. 3–39, 2000.
[34] G. S. Fishman, *Monte Carlo: Concepts, Algorithms, and Applications*. Berlin, Germany: Springer, 2013, pp. 493–583.
[35] A. Haldar and S. Mahadevan, "First-order and second-order reliability methods," *Probabilistic Structural Mechanics Handbook*. Boston, MA, USA: Springer, 1995.
[36] H. Solomon and M. A. Stephens, "Approximations to density functions using pearson curves," *J. Amer. Statist. Assoc.*, vol. 73, pp. 153–160, Mar. 1978.
[37] K. Sobczyk and J. Trcebicki, "Approximate probability distributions for stochastic systems: Maximum entropy method," *Comput. Methods Appl. Mech. Eng.*, vol. 168, no. 168, pp. 91–111, 1999.
[38] K. Breitung, "Probability approximations by log likelihood maximization," *J. Eng. Mech.*, vol. 117, no. 3, pp. 457–477, 1991.
[39] R. Fletcher, *Practical Methods of Optimization*. Hoboken, NJ, USA: Wiley, 2013, pp. 127–156.
[40] J. K. Sim, S. Yoon, and Y.-H. Cho, "Wearable sweat rate sensors for human thermal comfort monitoring," *Sci. Rep.*, vol. 8, no. 1, 2018, Art. no. 1181.
[41] J. F. Tressler, S. Alkoy, and R. E. Newnham, "Piezoelectric sensors and sensor materials," *J. Electroceram.*, vol. 2, no. 4, pp. 257–272, 1998.
[42] J. G. Smits, S. I. Dalke, and T. K. Cooney, "The constituent equations of piezoelectric bimorphs," *Sens. Actuators A, Phys.*, vol. 28, no. 1, pp. 41–61, 1991.
[43] A. Spivak, A. Belenky, and O. Yadid-Pecht, "Very sensitive low-noise active-reset CMOS image sensor with in-pixel ADC," *IEEE Trans. Circuits Syst. II, Exp. Briefs*, vol. 63, no. 10, pp. 939–943, Oct. 2016.

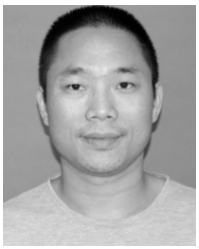

Z. L. HUANG received the Ph.D. degree from Hunan University, China, in 2017. He was an Associate Professor with the School of Mechanical and Electrical Engineering, Hunan City University. His current research interests include the reliability modeling and robust design optimization for sensors, and the multiphysics coupling analysis for electromechanical equipments.

J. W. ZHANG is currently pursuing the bachelor's degree with the School of Mechanical and Electrical Engineering, Hunan City University, China. He is currently an Assistant Researcher with the Smart City Research Institute, Hunan Province.

TARUN KUMAR is currently pursuing the bachelor's degree with the Department of Electronics and Electrical Communication Engineering, IIT Kharagpur, where he has worked in biomedical devices and bioelectronics instrumentation with the Bioelectronics Innovation Laboratory and National MEMS Laboratory.

T. G. YANG received the Ph.D. degree from Central South University, China, in 2013. He was a Professor with the School of Mechanical and Electrical Engineering, Hunan City University. His current research interests include the grid-connected inverters control for new energy, fault diagnosis for induction motor.

S. G. DENG received the Ph.D. degree from Southeast University, China, in 2012. He was a Professor with the Smart City Research Institute, Hunan City University. His current research interests include sensor networks and laser communication.

F. Y. LI received the Ph.D. degree from Hunan University, China, in 2009. He was an Associate Professor with the School of Automotive and Mechanical Engineering, Changsha University of Science and Technology. His current research fields include structural reliability analysis and design optimization, multi-physical coupling analysis, and multi-disciplinary optimization design.